RSC Advances

PAPER

View Article Online
View Journal | View Issue

Cite this: *RSC Adv.*, 2018, **8**, 38140

Expansion of the photoresponse window of a $BiVO_4$ photocatalyst by doping with chromium(VI)†

Kazuya Okuno,[a] Hideki Kato,*[a] Junie Jhon M. Vequizo,[b] Akira Yamakata,*[b] Hisayoshi Kobayashi,[c] Makoto Kobayashi[a] and Masato Kakihana[a]

Received 20th September 2018
Accepted 2nd November 2018

DOI: 10.1039/c8ra07830k

rsc.li/rsc-advances

Doping of Cr^{6+} into $BiVO_4$ was examined in this study. A new absorption band with a 1.84 eV energy threshold appeared with Cr-doping. The theoretical band calculation has revealed that the new absorption is ascribed to the electron transition from the valence band to acceptor levels formed by empty Cr 3d orbitals. It was confirmed that photocatalytic water oxidation in the presence of Ag^+ or Fe^{3+} of an oxidizing reagent was induced by excitation of the new absorption although activity under band gap excitation decreased with Cr-doping. Characteristics of carrier dynamics were also investigated by transient absorption spectroscopy.

1. Introduction

Much attention has been paid to photocatalytic water splitting into H_2 and O_2 as one candidate method for solar hydrogen production.[1,2] Although highly efficient water splitting has been achieved under ultraviolet irradiation,[1–4] a visible-light response is highly demanded from the viewpoint of solar H_2 production. Overall water splitting under visible light by suspended single photocatalyst systems has been achieved, but their efficiencies are still low.[5,6] The Z-scheme system composed of two kinds of photocatalysts bringing about either H_2 or O_2 evolution is another strategy for photocatalytic water splitting under visible light.[7] One of the merits of the Z-scheme system is that water splitting can be achieved by utilization of photocatalysts incapable of water splitting themselves. Monoclinic $BiVO_4$ with a scheelite structure (ms-$BiVO_4$) is one of the representative O_2-evolving photocatalysts for the Z-scheme systems.[7,8] ms-$BiVO_4$ can be combined with many kinds of H_2-evolving photocatalysts, such as $SrTiO_3$:Rh, $CuGaS_2$, Cu_2ZnGeS_4, CdS, $LaMg_{1/3}Ta_{2/3}O_2N$ and $La_5Ti_2CuS_5O_7$, to achieve Z-scheme water splitting.[9–15] It is noteworthy that particulate ms-$BiVO_4$ is used in photocatalyst sheets giving 1.1–1.2% solar-to-hydrogen energy conversion efficiencies.[10,11] Electrodes based on ms-$BiVO_4$ are also utilized as photoanodes for photoelectrochemical water splitting.[16–18] Thus, ms-$BiVO_4$ is an attractive visible-light-responsive photocatalyst for water oxidation. However, the development of photocatalysts working under longer wavelengths is still demanded because the photoresponse of ms-$BiVO_4$ up to 520 nm wavelength is not sufficient in terms of solar energy conversion.[19] A variety of attempts have so far been made to improve the performance of $BiVO_4$, especially its photoelectrochemical efficiency,[16–18,20–23] while there are no reports regarding extension of the photoresponse window of $BiVO_4$.

As some partially oxidized metal cations such as Pb^{2+}, Bi^{3+}, Ag^+, Sn^{2+} and Cu^+ are known as constituents to form valence bands (VBs) or electron donor levels at shallow potential in comparison with O^{2-}, these cations are used for visible light driven photocatalysts.[1,24] Nevertheless, formation of electron acceptor levels at a deeper (more positive) position than the conduction band (CB) seems to be effective in expanding the photoresponse window of ms-$BiVO_4$ rather than formation of electron donor levels because of the presence of a shallow VB by the contribution of Bi^{3+}. A hexavalent chromium ion is known as one candidate constituent to form electron acceptor levels or CB at deep potentials.[25,26] The Cr^{6+}-substitution for $PbMoO_4$ is a good example of narrowing the energy gaps of scheelite-type compounds.[25] In this study, substitution of Cr^{6+} for V^{5+} in ms-$BiVO_4$ was investigated with the aim of expanding the photoresponse window.

2. Experiments

2.1 Sample preparation

Powders of $BiV_{1-x}Cr_xO_4$ were synthesized by a liquid solid state reaction (LSR) method.[8] Raw materials of 20 mmol of $Bi(NO_3)_3 \cdot 5H_2O$ (Kanto, 99.9%), 9.5–10 mmol of V_2O_5 (Kanto, 99.0%) and 0–0.1 mmol of $CaCrO_4$ (Strem, 95%) were added to 30 ml of 0.1 mol l^{-1} HNO_3. The suspended solution was stirred

[a]*Institute of Multidisciplinary Research for Advanced Materials, Tohoku University, 2-1-1 Katahira, Aoba-ku, Sendai 980-8577, Japan. E-mail: hideki.kato.e2@tohoku.ac.jp*

[b]*Graduate School of Engineering, Toyota Technological Institute, 2-12-1 Hisakata, Tempaku-ku, Nagoya 468-8511, Japan. E-mail: yamakata@toyota-ti.ac.jp*

[c]*Department of Chemistry and Materials Technology, Graduate School of Science and Technology, Kyoto Institute of Technology, Sakyo-ku, Kyoto 606-8585, Japan*

† Electronic supplementary information (ESI) available: Transmittance spectra of optical filters used, XRD patterns of samples obtained, scanning electron microscopy images and a Tauc plot. See DOI: 10.1039/c8ra07830k

for 26–168 h in the dark under ambient conditions. The resulting precipitation was washed with 1 mol l^{-1} HNO_3 followed by distilled water, and was then dried at 80 °C for 5 h in air. Synthesis of the Cr-doped sample using Cr_2O_3 instead of $CaCrO_4$ was also conducted by the same manner for comparison.

2.2 Characterization

Crystal phases in the obtained samples were identified by X-ray diffraction (XRD; Bruker AXS, D2 PHASER). Photoabsorption spectra were taken by a diffuse reflection method using an ultraviolet-visible-near infrared (IR) spectrometer (Shimadzu, UV-3100) with an integrating sphere and obtained spectra were converted by the Kubelka–Munk method. Energy gaps of indirect transition in non-doped and Cr-doped samples were determined from the $(\alpha h\nu)^{1/2}$–$h\nu$ plot (Tauc plot for indirect transition), where α, h and ν represent the Kubelka–Munk function, Planck constant and frequency, respectively. The particles were observed by scanning electron microscopy (SEM; Hitachi, SU-1510). Specific surface areas were determined by N_2 adsorption and BET analysis (MicrotracBEL, BELSORP-miniII). Elemental compositions were analysed by inductively coupled plasma atomic emission spectroscopy (ICP-AES; SPECTRO, ARCOS EOP).

2.3 Photocatalytic reactions

Photocatalytic activity for O_2 evolution from an aqueous $AgNO_3$ (Kanto, 99.5%) solution was examined in a gas-closed circulation system with an on-line gas chromatograph (Shimadzu, GC-14B, TCD, MS-5A column, Ar carrier). Photocatalyst powder (0.1 g) was dispersed in 160 ml of a 0.02 mol l^{-1} aqueous $AgNO_3$ solution containing 0.1 g of La_2O_3 as a pH buffer to adjust the pH to around 8.5. Photocatalytic O_2 evolution from 2 mmol l^{-1} of an aqueous $Fe(ClO_4)_3$ (Kanto, 90%) solution, the pH of which was adjusted to 2.3 by $HClO_4$ (Kanto, 60%), was also examined. The photocatalyst was irradiated by a 300 W Xe arc lamp (Excelitas, Cermax PE300BF) with two kinds of conditions ($\lambda >$ 420 and 540 nm). The transmittance spectra of cut-off filters used are shown in Fig. S1†.

2.4 Theoretical calculations of band structures

The band structures were calculated by the plane wave based density functional theory (DFT) using the CASTEP program.[27,28] The Perdew–Burke–Ernzerhof (PBE) functional was used together with the ultrasoft-core potentials.[29–31] The cutoff energies were set to 300 eV. The electron configurations of the atoms were O: $2s^2 2p^4$, Ca: $3s^2 3p^6 4s^2$, V: $3s^2 3p^6 3d^3 4s^2$, Cr: $3s^2 3p^6 3d^4 4s^2$ and Bi: $6s^2 6p^3$. Super cells of $Bi_4V_4O_{16}$ and $Bi_{15}CaV_{15}CrO_{64}$ were employed as models of non-doped and Cr-doped $BiVO_4$. For the Cr-doped model, one Bi atom was also replaced with a Ca atom accompanied by the substitution of Cr for V to maintain the charge balance in the Cr-doped $BiVO_4$ system. The total numbers of electrons were 168 and 678 for $Bi_4V_4O_{16}$ and $Bi_{15}CaV_{15}CrO_{64}$, respectively. It was confirmed that transitions from the VB to CB minimum and from VB to the Cr 3d orbital are indirect.

2.5 Time resolved transient absorption measurements

The microsecond time-resolved visible to mid-IR absorption measurements were performed by using laboratory-built spectrometers as described in the previous paper.[32] Briefly, in the mid-IR region (6000–1000 cm^{-1}), the measurement was carried out in transmission mode, wherein the probe light emitted from a $MoSi_2$ coil was focused on the sample, and then the transmitted light was introduced to a grating spectrometer. The monochromated light was then detected by an MCT detector (Kolmar), and the output electric signal was amplified with an AC-coupled amplifier (Stanford Research Systems, SR560, 1 MHz). In the visible to near IR region (25 000–6000 cm^{-1}), the experiments were performed in the reflection mode, wherein the probe light that comes from a halogen lamp (50 W) was focused on the sample and detected using Si or InGaAs photodiodes. In each experiment, the pump ultraviolet laser pulses (355 nm) that originated from the Nd:YAG laser (Continuum, Surelite I, duration: 6 ns, power: 0.5 mJ, repetition rate: 10–0.01 Hz) were utilized to excite the samples. The time resolution of the spectrometers was limited to 1–2 μs by the bandwidth of the amplifier. To determine the decay processes and reactivity of photogenerated charge carriers, the measurements were performed in vacuum at room temperature.

3. Results and discussion

3.1 Synthesis of Cr-doped ms-$BiVO_4$

A single phase of ms-$BiVO_4$ was obtained in the non-doped sample after 26 h of reaction, while formation of the ms-$BiVO_4$ phase by the LSR slowly proceeded in the Cr(2%)-doped sample (Fig. S2†). At 26 h of reaction time, the Cr(2%)-doped sample was still a mixture of V_2O_5, $Bi_6O_5(OH)_3(NO_3)_5(H_2O)_3$ and a tiny amount of tetragonal $BiVO_4$ with a zircon structure (tz-$BiVO_4$). Even for the Cr(2%)-doped sample, the single phase of ms-$BiVO_4$ was eventually obtained with 100 h of reaction time and longer. Both samples with and without Cr-doping showed no changes in the intensity and width of diffraction peaks with a prolonged reaction time of up to 1 week. Synthesis of $BiVO_4$ with different amounts of Cr-doping (0.1–5%) was attempted by the LSR method with 1 week of reaction time (Fig. 1). The single phase of ms-$BiVO_4$ was obtained with up to 2% Cr-doping while mixtures of ms- and tz-$BiVO_4$ were obtained for samples with larger amounts of doping (3–5%). Synthesis of the pure phase of ms-$BiVO_4$ with Cr(3–5%) has not been achieved by the LSR method even with a further prolonged reaction time of up to 4 weeks. Doping with Cr resulted in no significant changes in the morphology and size of particles (Fig. S3†). Elemental analysis by ICP-AES proved that, in the samples obtained as the pure phase of ms-$BiVO_4$, the amounts of Cr incorporated in $BiVO_4$ increased with the increases in the intended values although actual values were slightly lower than the nominal ones (Table 1). The fact that the supernatant solution obtained after the synthesis of the Cr-doped sample was yellow due to the presence of Cr^{6+} ions also supported the slightly lower amounts of Cr in the

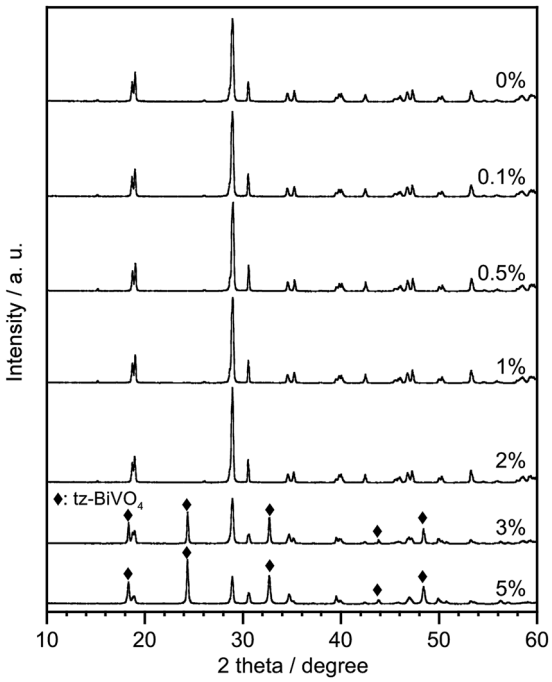

Fig. 1 XRD patterns of $BiVO_4$ doped with various amounts of Cr synthesized by the LSR method with 1 week of reaction time.

Table 1 Elemental composition determined by ICP-AES analysis

	Atomic composition			
Cr Content[a]/mol%	Bi	Ca	V	Cr
0	1	—	1.018	—
0.5	1	0	0.990	0.004
1	1	0	0.981	0.007
2	1	0	0.975	0.016
2[b]	1	0	1.024	0
3	1	0	1.024	0.025
5	1	0	1.099	0.016

[a] In the starting mixture. [b] Cr_2O_3 was used as the source of Cr.

obtained samples. In the substitution of aliovalent ions, that is, substitution of Cr^{6+} for V^{5+} in the present case, co-substitution of Ca^{2+} for Bi^{3+} was thought to be one kind of ideal charge compensation. However, the elemental analysis proved that such co-substitution of Ca did not occur and suggested the formation of V defects to keep the charge balance. The samples synthesized using Cr_2O_3 instead of $CaCrO_4$ were obtained as a pure phase of ms-$BiVO_4$, but no Cr was incorporated in the sample as shown in Table 1. The excessively large ionic radius of Cr^{3+} against V^{5+} is the reason for no substitution of Cr^{3+} into ms-$BiVO_4$ using the LSR method. No report of the ionic radius of Cr^{3+} in a 4-fold coordination in the paper by Shannon also supports the difficulty of substitution of Cr^{3+} for tetrahedral sites.[33] Thus, it is obvious that Cr ions incorporated into ms-$BiVO_4$ by the LSR method are not Cr^{3+} but Cr^{6+}.

3.2 Photoabsorption properties and band structure

The Cr-doped ms-$BiVO_4$ showed a new absorption band in addition to the intrinsic band gap excitation of ms-$BiVO_4$ as shown in Fig. 2. The intensity of the new absorption band became stronger as the amount of Cr doping increased. There are no doubts that chromium is responsible for the appearance of the low energy absorption band. It was expected that the new absorption could be attributed to electron transition from VB to acceptor levels formed by the empty 3d orbitals of Cr^{6+}. Theoretical calculations of band structures based on DFT were performed for super cells of $Bi_4V_4O_{16}$ and $Bi_{15}CaV_{15}CrO_{64}$ as models of non-doped and Cr-doped samples. Although the charge balance was kept not by Ca^{2+} ions but V^{5+} defects in the real samples, the co-substituted model was used to simplify the calculation. Fig. 3 depicts the projected density of states (PDOS) near the band gap of $Bi_4V_4O_{16}$ and $Bi_{15}CaV_{15}CrO_{64}$. The empty Cr 3d orbitals appeared below CB in $Bi_{15}CaV_{15}CrO_{64}$ and no other significant differences were seen between $Bi_4V_4O_{16}$ and $Bi_{15}CaV_{15}CrO_{64}$ in PDOS near the band gap. Thus, it has been proven that Cr^{6+} ions doped into ms-$BiVO_4$ form acceptor levels in the band gap and that the new absorption band is attributed to electron transition from the valence band to the acceptor levels formed by Cr^{6+} similar to Cr-doped $PbMoO_4$.[25] The threshold energy of the new absorption band was determined from the Tauc plot to be 1.86 and 1.84 eV for Cr(0.1%)- and Cr(0.5–2%)-doped samples (Fig. S4†) and this is narrower by 0.52–0.54 eV than the band gap energy of non-doped ms-$BiVO_4$ (2.38 eV). These experimental values are in good agreement with the theoretically calculated values, 1.59 and 2.23 eV for $Bi_4V_4O_{16}$ and $Bi_{15}CaV_{15}CrO_{64}$, although the theoretical values are slightly smaller than the experimental values as is usually observed. Moreover, a 1.84 eV energy gap is narrower than those of other Cr^{6+}-containing photocatalysts, $PbMoO_4$:Cr (2.26 eV) and $PbCrO_4$ (2.3 eV).[25,26]

3.3 Photocatalytic activity

Table 2 summarizes the photocatalytic activities of Cr-doped ms-$BiVO_4$ for the O_2 evolution reaction using Ag^+ as an oxidizing reagent. Two kinds of irradiation conditions were examined to see photocatalytic activity induced by the excitation

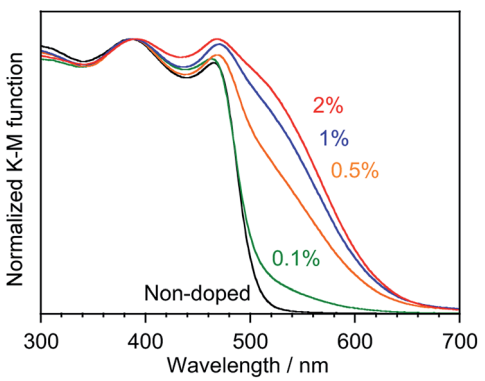

Fig. 2 Absorption spectra of Cr-doped ms-$BiVO_4$.

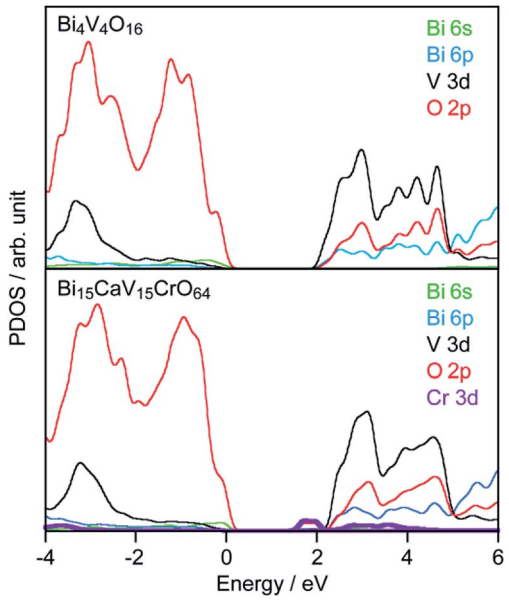

Fig. 3 PDOS of $Bi_4V_4O_{16}$ and $Bi_{15}CaV_{15}CrO_{64}$.

Table 2 Photocatalytic activity of Cr-doped ms-$BiVO_4$[a]

		O_2 evolution/μmol h^{-1}	
Cr/mol%	S_{BET}/m^2 g^{-1}	λ > 420 nm	λ > 540 nm
0	1.1	5.9	0.2
0.1	1.1	2.2	0.3
0.5	1.3	1.7	0.4
1.0	1.1	2.5	0.5
2.0	1.5	3.5	0.9

[a] Catalyst: 0.1 g, reactant solution: 0.02 mol l^{-1} $AgNO_3$ with 0.1 g of La_2O_3, light source: 300 W Xe lamp.

of the new absorption band. Whole visible light (λ > 420 nm) enables band gap excitation while a portion of the longer wavelength side of visible light (λ > 540 nm) is insufficient for band gap excitation but enables excitation of the new absorption. Indeed, the rate of O_2 evolution over non-doped ms-$BiVO_4$ was very low under the long wavelength light irradiation. Activity under whole visible light decreased with doping with Cr up to 0.5% and then increased with further doping while activity under the long wavelength light irradiation was monotonically increased with the amount of Cr. It has been reported that large particles are favorable for O_2 evolution with it being a 4-electron reaction.[34] However, such effects of the particle size were negligible in the present samples possessing similar particle sizes of around 1.5 μm and the almost constant specific surface area (S_{BET}) of 1.3 ± 0.2 m^2 g^{-1}. The improvements of the activity induced by excitation of the new absorption are due to enhancement of absorption with the amount of Cr doping. It was also confirmed that Cr(2%)-doped ms-$BiVO_4$ produced O_2 from an aqueous $Fe(ClO_4)_3$ solution (2 mmol l^{-1}, pH 2.3) at a rate of 0.14 μmol h^{-1} under long wavelength light irradiation despite there being no O_2 evolution over non-doped ms-$BiVO_4$. The results described above prove that the carriers photogenerated by excitation of the new absorption band, electrons in acceptor levels formed by empty Cr 3d and holes in VB, are available for photocatalytic water oxidation reactions using oxidizing reagents despite low activity; 0.06% and 0.03% apparent quantum yields for O_2 evolution over a Cr(2%)-doped sample from $AgNO_3$ at 540 and 580 nm, respectively.

3.4 Transient absorption analysis

Doping with foreign elements frequently decreases photocatalytic activity due to enhancement of carrier recombination by dopants.[35] Transient absorption measurements were performed to analyse carrier dynamics. Fig. 4 shows transient absorption spectra of non-doped and Cr(2%)-doped ms-$BiVO_4$ taken under vacuum. It is known that transient absorption owing to trapped holes appears near the band gaps whereas deeply trapped electrons give absorption at 5000–19 000 cm^{-1}.[32] Non-doped ms-$BiVO_4$ gave two obvious kinds of absorption bands ascribed to trapped holes at 18 000–21 000 cm^{-1} and deeply trapped electrons at 6000–18 000 cm^{-1}. In addition, absorption ascribed to free and/or shallowly trapped electrons, which is usually observed at lower energy than 5000 cm^{-1}, was very weak in non-doped ms-$BiVO_4$. Cr(2%)-doped ms-$BiVO_4$ showed three different features in the transient absorption spectra in comparison with the non-doped sample. (1) The absorption attributed to trapped holes remarkably shifted to 15 600 cm^{-1} in the Cr(2%)-doped sample accompanied with a lower energy gap (threshold energy: 14 840 cm^{-1}). (2) The shape of absorption for deeply trapped electrons was changed by Cr-doping and three obvious bands were seen at 9400, 11 000

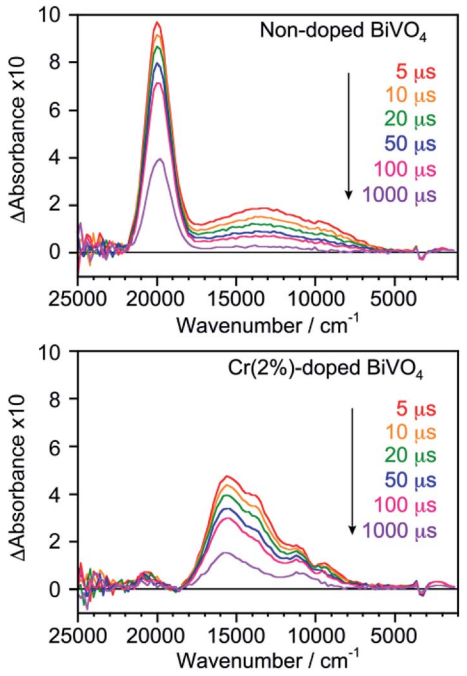

Fig. 4 Transient absorption spectra of non-doped and Cr(2%)-doped ms-$BiVO_4$ taken under vacuum.

and 13 600 cm^{-1}. (3) The absorption at the lowest energy side attributed to free or shallowly trapped electrons slightly increased by doping with Cr^{6+}. The significant changes in the structure of transient absorption relating to the deeply and shallowly trapped electrons could be caused by the electron acceptor levels formed by Cr^{6+} ions and/or the V^{5+} defects. Decay curves of shallowly trapped electrons at 4500 cm^{-1}, deeply trapped electrons at 11 000 cm^{-1} and trapped holes at 20 000 and 15 600 cm^{-1} for non-doped and Cr(2%)-doped ms-$BiVO_4$ are presented in Fig. 5. The shallowly trapped electrons monitored at 4500 cm^{-1} slowly decreased in the Cr(2%)-doped sample compared to the non-doped one. The decay curves at 11 000 cm^{-1} indicated that the deeply trapped electrons also decreased faster in the non-doped sample than in the Cr(2%)-doped one. Both samples showed almost the same slope in the decay curves for trapped holes, where it should be noted that the direct comparison of absorbance between the samples was difficult because of the remarkable difference in the peak positions. These carrier dynamics analyses prove that Cr^{6+} ions doped into ms-$BiVO_4$ do not dominantly facilitate the recombination of electrons and holes despite formation of electron traps.

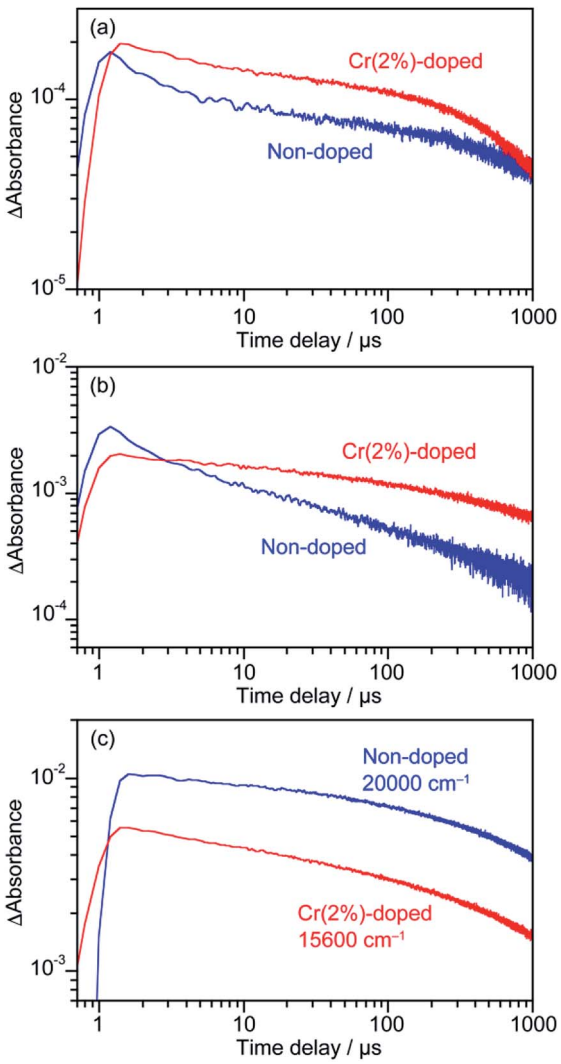

Fig. 5 Decay curves of transient absorption of non-doped and Cr(2%)-doped ms-$BiVO_4$ monitored at (a) 4500 cm^{-1}, (b) 11 000 cm^{-1} and (c) 20 000 and 15 600 cm^{-1}, respectively.

4. Conclusions

It has been confirmed that substitution of Cr^{6+} for V^{5+} in ms-$BiVO_4$ is possible by the LSR method. The Cr-doping results in the appearance of a new absorption band with a 1.84 eV energy threshold. Photocatalytic O_2 evolution can be induced by excitation of the new absorption band. Thus, it has been demonstrated that doping with Cr^{6+} ions is a way of expanding the photoresponse window of ms-$BiVO_4$. Transient carrier dynamics analyses indicate that decreases in the photocatalytic activity by doping with Cr^{6+} are not due to enhanced carrier recombination and suggest that the low mobility of electrons in the discrete deep traps (empty Cr 3d) limits the activity at this time. It implies the possibility of further improvements of activity by modification. O_2 evolution using Fe^{3+} as an electron acceptor suggests the possibility of applying Cr-doped ms-$BiVO_4$ to Z-scheme systems after some improvements.

Conflicts of interest

There are no conflicts to declare.

Acknowledgements

This study was partly supported by KAKENHI Grant Numbers JP16H04186, JP16H04188 and JP17H05491 and Dynamic Alliance for Open Innovation Bridging Human, Environment and Materials.

References

1 A. Kudo and Y. Miseki, *Chem. Soc. Rev.*, 2009, **38**, 253.
2 X. Chen, S. Shen, L. Guo and S. Mao, *Chem. Rev.*, 2010, **110**, 6503.
3 Y. Sakata, Y. Matsuda, T. Nakagawa, R. Yasunaga, H. Imamura and K. Teramura, *ChemSusChem*, 2010, **4**, 181.
4 Y. Ham, T. Hisatomi, Y. Goto, Y. Moriya, Y. Sakata, A. Yamakata, J. Kubota and K. Domen, *J. Mater. Chem. A*, 2016, **4**, 3027.
5 C. Pan, T. Takata, M. Nakabayashi, T. Matsumoto, N. Shibata, Y. Ikuhara and K. Domen, *Angew. Chem., Int. Ed.*, 2015, **54**, 295.
6 W. Liu, L. Cao, W. Cheng, u. Cao, X. Liu, W. Zhang, Z. Mou, L. Jin, X. Zheng, W. Che, Q. Liu, T. Yao and S. Wei, *Angew. Chem., Int. Ed.*, 2017, **56**, 9312.
7 K. Maeda, *ACS Catal.*, 2013, **3**, 1486.
8 A. Kudo, K. Omori and H. Kato, *J. Am. Chem. Soc.*, 1999, **121**, 11459.
9 H. Kato, Y. Sasaki, N. Shirakura and A. Kudo, *J. Mater. Chem. A*, 2013, **1**, 12327.
10 Q. Wang, T. Hisatomi, Q. Jia, H. Tokudome, M. Zhong, C. Wang, Z. Pan, T. Takata, M. Nakabayashi, N. Shibata,

Y. Li, I. D. Sharp, A. Kudo, T. Yamada and K. Domen, *Nat. Mater.*, 2016, **15**, 611.
11 Q. Wang, T. Hisatomi, Y. Suzuki, Z. Pan, J. Seo, M. Katayama, T. Minegishi, H. Nishiyama, T. Takata, K. Seki, A. Kudo, T. Yamada and K. Domen, *J. Am. Chem. Soc.*, 2017, **139**, 1675.
12 A. Iwase, S. Yoshino, T. Takayama, Y. H. Ng, R. Amal and A. Kudo, *J. Am. Chem. Soc.*, 2016, **138**, 10260.
13 Z. Pan, T. Hisatomi, Q. Wang, S. Chen, M. Nakabayashi, N. Shibata, C. Pan, T. Takata, M. Katayama, T. Minegishi, A. Kudo and K. Domen, *ACS Catal.*, 2016, **6**, 7188.
14 Y.-J. Yuan, D. Chen, S. Yang, L.-X. Yang, J.-J. Wang, D. Cao, W. Tu, Z.-T. Yu and Z.-G. Zou, *J. Mater. Chem. A*, 2017, **5**, 21205.
15 S. Sun, T. Hisatomi, Q. Wang, S. Chen, G. Ma, J. Liu, S. Nandy, T. Minegishi, M. Katayama and K. Domen, *ACS Catal.*, 2018, **8**, 1690.
16 K. Sayama, A. Nomura, T. Arai, T. Sugita, R. Abe, M. Yanagida, T. Oi, Y. Iwasak, Y. Abe and H. Sugihara, *J. Phys. Chem. B*, 2006, **110**, 11352.
17 F. F. Abdi, L. Han, A. H. M. Smets, M. Zeman, B. Dam and R. van de Krol, *Nat. Commun.*, 2013, **4**, 2195.
18 T. W. Kim and K.-S. Choi, *Science*, 2014, **343**, 990.
19 K. Maeda and K. Domen, *J. Phys. Chem. Lett.*, 2010, **1**, 2655.
20 S. J. Hong, S. Lee, J. S. Jang and J. S. Lee, *Energy Environ. Sci.*, 2011, **4**, 1781.
21 R. Li, F. Zhang, D. Wang, J. Yang, M. Li, J. Zhu, X. Zhou, H. Han and C. Li, *Nat. Commun.*, 2013, **4**, 1432.
22 R. Li, H. Han, F. Zhang, D. Wang and C. Li, *Energy Environ. Sci.*, 2014, **7**, 1369.
23 Z. Jiang, Y. Liu, T. Jing, B. Huang, X. Zhang, X. Qin, Y. Dai and M.-H. Whangbo, *J. Phys. Chem. C*, 2016, **120**, 2058.
24 I. Sullivan, B. Zoellner and P. A. Maggard, *Chem. Mater.*, 2016, **28**, 5999.
25 Y. Shimodaira, H. Kato, H. Kobayashi and A. Kudo, *Bull. Chem. Soc. Jpn.*, 2007, **80**, 885.
26 Y. Miseki, O. Kitao and K. Sayama, *RSC Adv.*, 2015, **5**, 1452.
27 M. C. Payne, M. P. Teter, D. C. Allan, T. A. Arias and J. D. Johnnopoulos, *Rev. Mod. Phys.*, 1992, **64**, 1045.
28 V. Milman, B. Winkler, J. A. White, C. J. Pickard, M. C. Payne, E. V. Akhmatskaya and R. H. Nobes, *Int. J. Quantum Chem.*, 2000, **77**, 895.
29 D. Vanderbilt, *Phys. Rev. B*, 1991, **43**, 6796.
30 J. P. Perdew, K. Burke and M. Ernzerhof, *Phys. Rev. Lett.*, 1996, **77**, 3865.
31 J. P. Perdew, K. Burke and M. Ernzerhof, *Phys. Rev. Lett.*, 1997, **78**, 1396.
32 A. Yamakata, J. J. M. Vequizo and H. Matsunaga, *J. Phys. Chem. C*, 2015, **119**, 24538.
33 R. D. Shannon, *Acta Crystallogr.*, 1976, **A32**, 751.
34 F. Amano, E. Ishinaga and A. Yamakata, *J. Phys. Chem. C*, 2013, **117**, 22584.
35 T. Ikeda, T. Nomoto, K. Eda, Y. Mizutani, H. Kato, A. Kudo and H. Onishi, *J. Phys. Chem. C*, 2008, **112**, 1167.